Scheme I

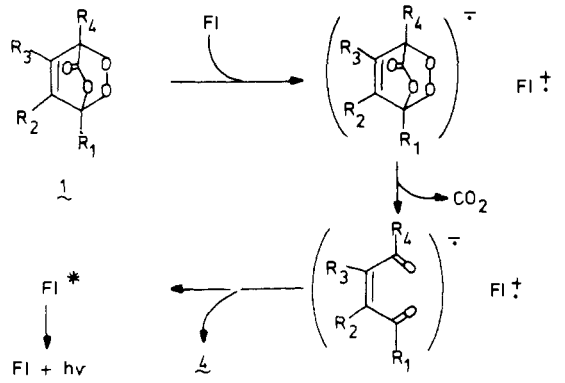

Discussion

Our results clearly indicate an electron-exchange mechanism for the fluorescer-enhanced chemiluminescence. On the one hand, a fluorescer like rubrene catalyzes the decarboxylation of the α-pyrone endoperoxide **1** with concurrent light amplification; on the other hand, the enhanced emission intensity is an exponential function of the oxidation potential of the fluorescers. Both criteria together are taken as evidence for the CIEEL mechanism.[13]

It was not possible to trap the *o*-dioxin **3** in the thermal decarboxylation of **1** even with such reactive dienophiles as 4-phenyl-1,2,4-triazoline-3,5-dione. Either **3** is not formed or it suffers valence isomerization to the diacylethylene **4** before bimolecular trapping with the dienophile occurs. If the latter situation should apply, it would also be unlikely that bimolecular electron exchange between the *o*-dioxin **3** and the fluorescer would compete with valence isomerization into **4**. This expectation is especially reasonable since the concentration of the triazolinedione trapping agent is fivefold that of the fluorescer electron donor. Furthermore, the fluorescer catalyzes the decarboxylation of the endoperoxide **1**, i.e., **1** disappears faster in the presence of rubrene. This is contrary to the observation made for the benzo-annulated endoperoxide (eq 3), for which the fluorescer does not directly catalyze the decarboxylation of the endoperoxide.

On the basis of our results we suggest the electron exchange mechanism shown in Scheme I to rationalize the enhanced chemiluminescence of α-pyrone endoperoxides **1** with easily oxidized fluorescers. Apparently the electron transfer between **1** and the fluorescer in the first step is quite inefficient since the catalyzed decomposition of **1** by Fl is slow and thus the enhanced light yield low.

Presently we are exploring the possibility of altering the structure of the endoperoxide **1** to increase the enhanced light efficiency by affording the intriguing *o*-dioxins **3**. For example, benzoannulation (eq 3) is very effective in enhancing the light yield by promoting the formation of the xylylene peroxide **5a**,[6] and the latter enters into an efficient electron-exchange mechanism. In the case of our α-pyrone endoperoxides **1** it seems that decarboxylation takes place concurrently with peroxide bond cleavage to afford **4** directly without the intervention of the *o*-dioxin **3**.

Acknowledgments are made to the donors of the Petroleum Research Fund, administered by the American Chemical Society, the National Science Foundation (CHE-78-12621), and the National Institutes of Health (GM-21119-03, GM-00141-04, and RR-8102-07).

References and Notes

(1) Part 86 in the Cyclic Peroxide series.
(2) NIH Career Development Awardee (1975–1980).
(3) Adam, W.; Erden, I. *Angew. Chem.* **1978**, *90*, 223.
(4) Adam, W. *Adv. Heterocycl. Chem.* **1977**, *21*, 437.
(5) Benson, S. W. "Thermochemical Kinetics", 2nd ed.; Wiley-Interscience: New York, 1976.
(6) Smith, J. P.; Schuster, G. B. *J. Am. Chem. Soc.* **1978**, *100*, 2564.
(7) Michl, J. *Photochem. Photobiol.* **1977**, *25*, 141.
(8) Mitchell, G. W.; Hastings, J. W. *Anal. Biochem.* **1971**, *39*, 243.
(9) Adam, W.; Simpson, G. A.; Yany F. *J. Phys. Chem.* **1974**, *78*, 2559.
(10) Diels, O.; Alder, K. *Justus Liebigs Ann. Chem.* **1931**, *490*, 257.
(11) Although we experienced no explosions in working with these labile peroxides, utmost *caution* should be exercised and all safety measures should be taken in handling these potentially hazardous substances. They should be stored in the freezer as dilute solutions rather than pure form to extend their lifetime.
(12) Ried, W.; Lim, S.-H. *Justus Liebigs Ann. Chem.* **1973**, 129.
(13) Koo, J.-Y.; Schuster, G. B. *J. Am. Chem. Soc.* **1978**, *100*, 4496.
(14) Weller, A.; Zachariasse, K. "Molecular Luminescence", Lim, E. C., Ed.; W. A. Benjamin: New York, 1969.

Multiphase Fluorescence Quenching by a Surfactant Nitroxyl Radical

Samir S. Atik, C. L. Kwan, and Lawrence A. Singer*

Contribution from the Department of Chemistry, University of Southern California, Los Angeles, California 90007. *Received March 22, 1979*

Abstract: The self-association of 4-[*N*,*N*-dimethyl-*N*-(*n*-hexadecyl)ammonium]-2,2,6,6-tetramethylpiperidinyl-*N'*-oxyl bromide (**1**), a surfactant nitroxyl radical, into micelles was studied by ESR spectroscopy giving an estimate of its critical micelle concentration (cmc) as $(4.6 \pm 0.5) \times 10^{-4}$ M, in the absence of added salt. The fluorescence quenching of a series of cationic fluorophors of the structure $[(1\text{-pyrenyl})(CH_2)_nN(CH_3)_3]^+ X^-$ (**2**-*n*) by **1** was investigated over a concentration range below and above the cmc. A comparison of fluorescence lifetime and yield measurements indicates that **2**-1 and **2**-5 are quenched by a simple diffusional mechanism while **2**-11 is quenched by a static mechanism below the cmc. Discontinuities occur in the Stern–Volmer plots at the cmc owing to the onset of static quenching of fluorophors solubilized in the micelle phase. Analysis of a kinetic scheme incorporating the several quenching mechanisms operating below and above the cmc leads to estimates of K_b/N for the **2**-*n* fluorophors: (**2**-1), 27; (**2**-5), 336; (**2**-11), 38 000 M^{-1}, where K_b is the association constant with the micelle and N is the aggregation number of the host micelle.

The study of bilayer and micellar assemblies with fluorescence probes is well established.[1] Recently, we[2] showed the usefulness of using nitroxyl radicals as fluorescence quenchers[3] in ionic micellar environments. Further, we have presented a

0002-7863/79/1501-5696$01.00/0

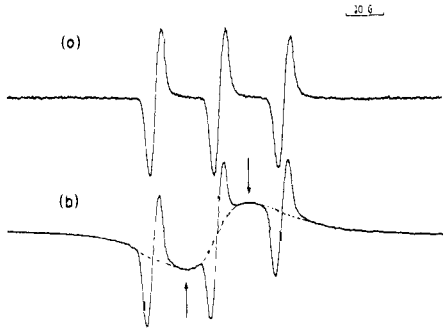

Figure 1. ESR spectra of **1**-Br in water under nondegassed conditions at modulation amplitude of 2.0 G: (a) at 6.0×10^{-5} M, (b) at 9.0×10^{-4} M in presence of 9.2×10^{-3} M KBr.

kinetic model for such systems, based on substrate binding via a multistep equilibrium, that is consistent with the often observed (a) upward curvature in steady-state Stern-Volmer plots and (b) the biexponential decay of the probe fluorescence.[4]

The present work describes the fluorescence quenching of several cationic pyrene derivates (**2**) by the surfactant nitroxyl

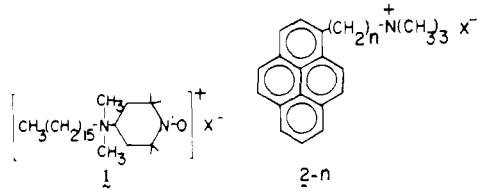

1 **2**-n

radical 4-[*N*,*N*-dimethyl-*N*-(*n*-hexadecyl)ammonium]-2,2,6,6-tetramethylpiperidinyl-*N'*-oxyl (**1**) over a concentration range below and above the critical micelle concentration (cmc) of the latter. The self-association of **1**-Br into micelles is studied by ESR spectroscopy,[5] yielding an estimate of its cmc that agrees well with observations in the fluorescence quenching experiment. This study elucidates the several fluorescence quenching mechanisms[6] operating below and above the cmc of the surfactant nitroxyl radical.

Results and Discussion

ESR Study of the Self-Association of 1-Br. The ESR spectrum of 1.0×10^{-5} M **1**-Br in water at 25 °C shows the characteristic nitroxyl radical three principal line pattern of 1.7 G width and $a_N = 16.9$ G.[5a] Additional hyperfine structure (~0.5 G) is observed in oxygen-free solutions at low modulation amplitude.[5b] At concentrations $>5 \times 10^{-4}$ M, the spectrum consists of a single, broad line (~15 G) superpositioned over the narrower three-line spectrum as shown in Figure 1. We assign the broad, single line spectrum to aggregates of **1**-Br where fast spin exchange occurs.

Because of the low amplitude of the broadened signal in the region of the low-field line in the spectrum of monomeric **1**-Br, the contribution of the former to peak-to-peak intensity measurements on the latter is estimated to be ≤5% in most of our experiments. Thus, monomeric [**1**-Br] can be directly monitored by intensity measurements on the low-field line.

The broadened, aggregate signal contour does not appear to vary with surfactant concentration and its intensity was monitored by peak-to-peak measurements at 7.5 G below and above (arrows in Figure 1) the monomer middle-field line where intensity contributions from the latter are negligible. *Thus, both monomer and aggregate* **1**-*Br can be simultaneously monitored in the ESR experiment.*

Plots of monomer and aggregate signal intensities vs. total [**1**-Br] are shown in Figure 2. In Figure 2a, aggregation is readily noted through the sharp discontinuity in the monomer

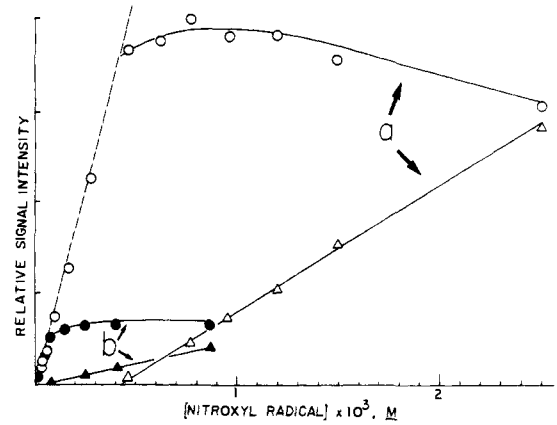

Fiure 2. Plots of relative peak-to-peak signal intensity vs. the concentration of surfactant nitroxyl radical **1**-Br: (a) in pure water, (○) monomer, (△) aggregate; (b) in presence of 9.2×10^{-3} M KBr, (●) monomer, (▲) aggregate. (---) Theoretical monome, spin intensity plot based on 4-keto-2,2,6,6-tetramethylpiperidinyl-*N*-oxyl as a standard.

profile and the development of the broadened, aggregate signal at $(4.6 \pm 0.5) \times 10^{-4}$ M which we assign as the critical micelle concentration (cmc) of **1**-Br.[7]

In the concentration range below the onset of the aggregate signal, the monomer signal profiles in Figures 2a and 2b are within 10% of the theoretical slopes (dashed lines) based on measurements relative to the signal intensity from 4-keto-2,2,6,6-tetramethylpiperidinyl-*N*-oxyl. However, we have observed that spin intensity measurements on very dilute solutions ($\leq 2 \times 10^{-5}$ M) of **1**-Br, in the absence or presence of O_2, are significantly *less* than theory. For example, peak-to-peak measurements of the low-field line indicate a spin intensity that is only ≃40% of the theoretical level at a concentration of 1.0×10^{-5} M. The spin intensity at this concentration is 100% of the theoretical level in the presence of 0.02 M cetyltrimethylammonium chloride which solubilizes and disperses the nitroxyl radical in the CTAC micelles.[5b]

Because of the apparently "normal" spin intensity measurements between 2×10^{-5} M and the cmc, we do not believe that this spin intensity loss is due to premicellar aggregation of the nitroxyl radicals in solution, since in that case the intensity loss would be enhanced with increasing concentration. At this time, we speculate that surface adsorption of the nitroxyl radicals, with accompanying severe peak broadening, is a possible explanation. Such a phenomenon would show a saturation limit as is observed and would be consistent with the effect of added CTAC. Since the surface tension measurements[7] indicate that only ~1% of the surfactant nitroxyl radicals are adsorbed at the water/air interface[8] under conditions of the ESR experiment, it is likely that the majority of the spin intensity loss arises from adsorption on the glass walls of the capillary tubes used in the ESR experiment which provides orders of magnitude more surface area than the water surface. The unexpected spin loss, and possibly related immobilization of a significant fraction of the surfactant nitroxyl radicals in very dilute solutions, does not jeopardize the results or conclusions in this or the earlier[5b] work which were carried out at higher concentrations.

In the presence of 0.0092 M potassium bromide, the cmc is lowered to $(8.5 \pm 0.5) \times 10^{-5}$ M (Figure 2b). The monomer intensity profile in the presence of 0.0050 M potassium bromide (not shown) shows a discontinuity at $(1.3 \pm 0.1) \times 10^{-4}$ M surfactant. The cmc's in the absence and presence of 0.0050 and 0.0092 M potassium bromide follow the expected log-log linear relationship[9] in eq 1, where the slope and intercept are least-square values.

$$\log (\text{cmc}) = -0.54 \log (\text{cmc} + [\text{KBr}]) - 5.1 \qquad (1)$$

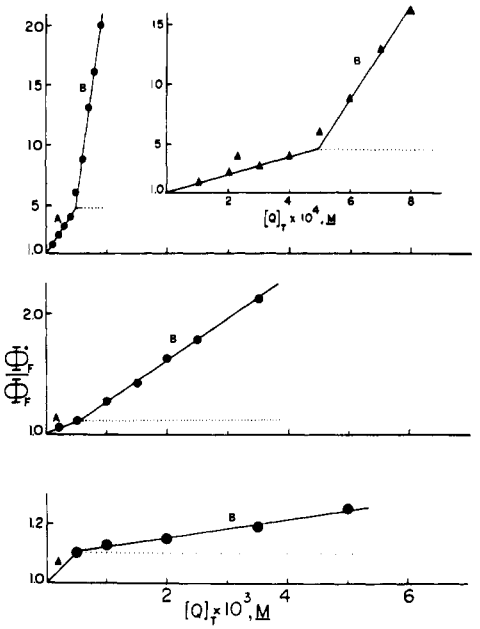

Figure 3. Stern-Volmer plots. (Upper) **2**-11, slopes: (region A) 7200 M^{-1}; (region B) 38 000 M^{-1}. (Inset) Expanded scale. (Middle) **2**-5, slopes: (region A) 220 M^{-1}; (region B) 370 M^{-1}. (Lower) **2**-1, slopes: (region A) 200 M^{-1}; (region B) 30 M^{-1}.

The decrease in monomer concentration above the cmc in Figure 1a is predicted by the law of mass action approach to micellization.[10] Qualitatively, this decrease results from a lowering of the cmc with increasing counterion concentration in accord with eq 1. Note that in the presence of 0.0050 and 0.0092 M potassium bromide, where $[Br^-]$ is approximately constant, the monomer intensity does not vary above the cmc (Figure 2b).

In the section that follows, we examine the fluorescence quenching of the cationic pyrene derivatives **2**-1, **2**-5, and **2**-11 by **1**.

Fluorescence Quenching of the Cationic Fluorophors. The emission from dilute ($\sim 10^{-5}$ M) aqueous solutions of **2**-1, **2**-5, or **2**-11 is very similar to the typical pyrene monomer spectrum. Fluorescence quenching of these fluorophors is observed as **1**-Br is added, but the data give unconventional Stern-Volmer plots as shown in Figure 3.

The fluorescence lifetimes of the **2**-*n* fluorophors, in the absence and presence of **1**-Br, appear in Table I. A very modest (5-10%) decrease in the lifetimes is noted as **1**-Br is added up to the cmc, but thereafter *the lifetimes show a tendency to lengthen with addition of quencher.*

For *diffusional* quenching[6] of an excited fluorophor (F*) by a quencher (Q), both the fluorescence lifetimes (eq 2) and fluorescence yields (eq 3) should decrease with added Q according to

$$\tau_{obsd}^{-1} = \tau_f^{-1} + k_q[Q] \quad (2)$$

and

$$\Phi_0/\Phi = 1 + k_q\tau_f[Q] \quad (3)$$

where τ_{obsd} and τ_f are the fluorescence lifetimes in the presence and absence of Q, k_q is the bimolecular rate constant for diffusional quenching, and Φ_0 and Φ are the fluorescence quantum yields in the absence and presence of Q. Accordingly, it is clear that much of the fluorescence quenching is not by a simple diffusional mechanism.

This dichotomy between the fluorescence yield and lifetime measurements is characteristic of static quenching.[6] Note that the steady-state quenching profiles in Figure 3 are discontinuous in the concentration region near the cmc of **1**-Br. We suggest that the Stern-Volmer slopes in region B primarily are due to *static quenching of fluorophors partitioned into the micelle phase.* Accordingly, in region B above the cmc, fluorescence is observed only from fluorophors residing in the aqueous phase. The tendency of the fluorescence lifetimes to *lengthen* slightly with added nitroxyl radical through this region is understandable since, in the absence of added salt, the concentration of monomeric **1**-Br in the aqueous phase, in fact, tends to decrease as noted in the ESR experiment.[12] An analysis of the Stern-Volmer data from region B is given later.

Table I. Fluorescence Lifetimes[a]

conditions	fluorophor, $\tau_f \times 10^9$, s[b]		
	2-1	**2**-5	**2**-11
pure water	51	102	99
water with **1**-Br, 2.5×10^{-4} M			90
5.0×10^{-4} M		95	87
1.0×10^{-3} M	46	95	87
2.0×10^{-3} M		97	
4.0×10^{-3} M		99	
5.0×10^{-3} M	46		90
1.0×10^{-2} M	48		
2.0×10^{-2} M	48		
water with 0.0050 M NaBr		99	

[a] Measured in 1-cm^2 Pyrex cuvettes under nondegassed conditions. Excitation at 337 nm with a nitrogen laser. [b] Multiple determinations with error limit of ±3%. Decays measured over two to three lifetimes.

Quenching below the cmc. The quenching mechanisms operating below the cmc (region A) can be elucidated to some degree by comparing the fluorescence yield and lifetime data. For **2**-5, the slope of 220 M^{-1} in region A, in combination with the $\tau_f = 102$ ns, leads to $k_q \approx 2 \times 10^9$ M^{-1} s^{-1} for a diffusional quenching mechanism (eq 3). This value agrees well with the estimate of $k_q \approx 1.4 \times 10^9$ M^{-1} s^{-1} which is derived from the decrease in the fluorescence lifetimes with added **1**-Br through region A (eq 2). We conclude that a diffusional mechanism accounts for the majority, if not all, of the quenching of **2**-5 below the cmc.

The apparent Stern-Volmer slope of ~200 M^{-1} in region A for **2**-1, and the $\tau_f = 51$ ns, indicates $k_q \approx 4 \times 10^9$ M^{-1} s^{-1}. This same value is indicated by the lifetime data, assuming that monomeric **1**-Br is present at its cmc for the entries in Table I. It appears that fluorescence quenching of **2**-1 below the cmc also can be associated with a diffusional mechanism.

The above type of analysis leads to a different conclusion for **2**-11. The Stern-Volmer slope of 7.2×10^3 M^{-1} in region A, along with the $\tau_f = 99$ ns, would require $k_q \approx 7 \times 10^{10}$ M^{-1} s^{-1}, which significantly exceeds the diffusion limit in water at room temperature. Further, the lifetime measurements, which presumably measure only the aqueous phase diffusional quenching, indicate $k_q \approx 4 \times 10^9$ M^{-1} s^{-1} with a related predicted Stern-Volmer slope for the steady-state experiment of only 400 M^{-1}. We conclude that the steady-state experiment below the cmc primarily is measuring *static quenching,*[13] implying some form of ground-state association between the fluorophor and quencher.

Additional evidence for such an interaction may be indicated in the electronic absorption spectra of **2**-11 in the absence and presence of **1**-Br. Upon addition of the surfactant nitroxyl radical in the concentration range $\sim 10^{-4}$ M, the spectrum of **2**-11 shows an increase in absorption as a shoulder near 355 nm. There is an abrupt loss of this red-shifted shoulder when the concentration of **1**-Br is approximately equal to its cmc. Further, there is a narrowing of all absorption bands of **2**-11 so that the extinction coefficients at the absorption maxima

increase significantly. The absorption spectrum is unchanged with addition of **1**-Br above the cmc except that contributions due to the spectrum of the nitroxyl radical become significant.

This same trend is noted when cetyltrimethylammonium choride (CTAC) is added as shown in Figure 4. Because CTAC is a nonquenching surfactant, it is possible to monitor the emission from the complexed fluorophor as well. These spectra (inset, Figure 4), which are all normalized to the monomer emission, reveal the development of a structureless emission (red-shifted from the highly structured monomer emission) as CTAC is added at concentrations below the cmc of the latter ($\sim 5 \times 10^{-3}$ M).[5b] This structureless emission tends to red shift as more CTAC is added. At and above the cmc, this emission is identical in wavelength with the well-known pyrene excimer emission.[11] As more CTAC is added, the intensity of the excimer emission decreases relative to the monomer emission.

We suggest that the red-shifted shoulder in the absorption spectra in Figure 4 is due to ground state interaction between two pyrene rings in an aggregate structure, and that the red-shifted structureless emission, even below the cmc of CTAC,[14] comes from pyrene excimers.[15] Note that, at the concentration of **2**-11 used in this experiment (2.5×10^{-5} M), excimers *cannot be formed by a diffusional mechanism* but rather must come from aggregates that include at least two fluorophors. These aggregates must contain at least one CTAC since the latter seems to promote the formation of excimers. The gradual red shift in the excimer emission with more added CTAC might reflect greater mobility of the pyrene chromophores within aggregate structures of increasing size that allows the excimers to reach the energetically preferred pyrene excimer geometry.[11,15] The decrease in excimer emission with added CTAC above the cmc is due to dilution, and eventual isolation, of **2**-11 among the CTAC micelles.

This same aggregation probably occurs between **2**-11 and **1**-Br except that all emission from these structures is statically quenched. At this time, we have no information on the size of these aggregate structures. Note that data obtained so far with **2**-1 and **2**-5 give no indication of similar aggregation, which probably reflects the importance of the hydrophobic interaction for this association.

Fluorescence Quenching above the cmc. As shown earlier, the discontinuities in the steady-state fluorescence quenching profiles of the three fluorophors by **1**-Br observed at, or near, the cmc are assigned to the onset of static quenching of the fluorophors solubilized in the micelle phase. In addition, the previous analysis indicates that diffusional quenching of **2**-1 and **2**-5, but static quenching of **2**-11, occurs below the cmc.

These several quenching pathways are incorporated into Scheme I. Micellization of **1** (Q in scheme) is given by step i. The association of the fluorophor (F) with Q to form smaller premicellar aggregates (Q·F) is given by ii. Note that Q·F represents an ensemble of aggregates which have not been elucidated in detail, and that K_c is only an apparent equilibrium constant. The association of F with the micelles (M_Q) is described by a multistep equilibrium (iii-v) which leads to an ensemble of micelles, $M_Q \cdot F_n$ ($n = 0, 1, 2 \ldots$). Steps vi-viii account for excitation of F distributed among $M_Q \cdot F_n$, F, and Q·F with χ_m, χ_a, and χ_c being the mole fractions of F in each of the three states. Steps ix and x describe the first-order decays ($k_1 = \tau_f^{-1}$) and diffusional quenching by Q of F* in the aqueous phase. The possible reversible association of F* with the micelles is provided by xi. Note that xi is important only *if* the rates of fluorescence decay of F* in the aqueous and micellar phases are comparable to, or slower than, $k_{mq}[M_Q]$ and k_{-mq}, respectively.

A few observations and comments would be helpful before proceeding further. Static quenching of excited fluorophors

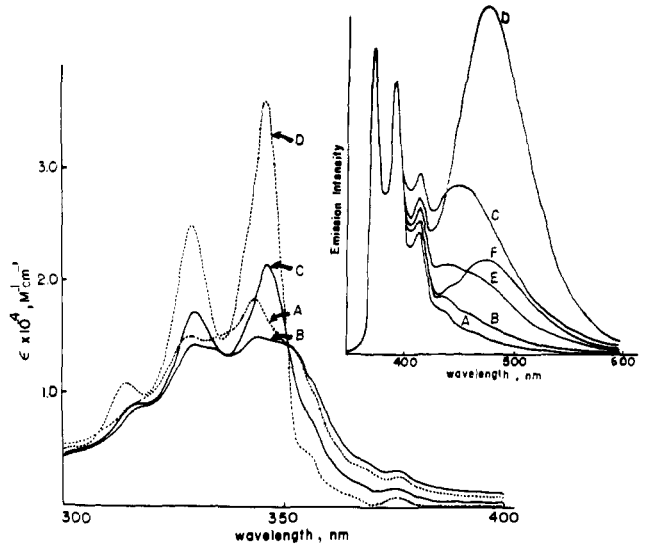

Figure 4. Absorption and emission spectra of 2.5×10^{-5} M **2**-11 in aqueous solutions in the absence and presence of CTAC. Concentrations of CTAC: (A) 0, (B) 1.0×10^{-3}, (c) 4.0×10^{-3}, (D) 5.0×10^{-3}, (E) 3.0×10^{-3}, (F) 6.0×10^{-3} M.

in the micelle phase implies that Nk_q' is faster than all other processes potentially available to the excited fluorophor including radiative and nonradiative decays as well as dissociation from the micelle (k_{mq}).[16] In agreement, only simple exponential decays are observed below and above the cmc. The latter is informative because more complex decays could arise from either (a) mixed fluorescences from aqueous and micelle phase solubilized excited fluorophors or (b) fluorescence only from aqueous phase fluorophors but with some contribution by

$$M_Q \cdot F^* \xrightarrow{k_{-mq}} M_Q + F^*$$

Static quenching of $M_Q \cdot F^*$ precludes both a and b.

Diffusional encounter between F* and the micelle is not important because the fluorescence lifetimes do not decrease with added Q above the cmc where $[M_Q]_T$ (the total concentration of micelles) increases according to $[M_Q]_T = \{[Q]_T - \text{cmc}\}/N$ with $[Q]_T$ being the total concentration of Q and N being the aggregation number for the micelle. If a reasonable value for N is assumed,[17] $[M_Q]$ is $\sim 10^{-5}$ M under the experimental conditions.

Based on Scheme I, but with the omission of step xi, the derivation in the Appendix leads to the Stern-Volmer expression

$$(\Phi_0/\Phi) = (1 + K_c[Q] + K_b[M_Q]_T)(1 + k_q\tau_f[Q]) \quad (4)$$

where [Q] is the concentration of monomeric Q and $[M_Q]_T$ is the concentration of micelles.

For the limiting case where $K_c[Q]$ and $K_b[M_Q]_T \ll 1$, meaning that both static quenching mechanisms are insignificant, (4) simplifies to (3). This case is observed with **2**-1 and **2**-5 below the cmc.

For these same two fluorophors above the cmc, static quenching by M_Q competes with diffusional quenching. This case is described by (5) which is a simplification of (4). Note that, above the cmc, the diffusional quenching term ($k_q\tau_f$cmc) is a constant, and the onset for eq 5 as the defining Stern-Volmer relationship is at $[Q]_T$ = cmc which is readily observed as a point of discontinuity in the Stern-Volmer plots for **2**-1 and **2**-5.

$$(\Phi_0/\Phi) = (1 + k_q\tau_f\text{cmc})(1 + K_b\{[Q]_T - \text{cmc}\}/N) \quad (5)$$

Scheme I

(i) $nQ \longrightarrow M_Q$	micellization of Q
(ii) $F + Q \overset{K_c}{\rightleftharpoons} Q{\cdot}F$	ground-state association of F with Q
(iii) $F + M_Q \underset{k_{-b}}{\overset{k_b}{\rightleftharpoons}} M_Q{\cdot}F$	multistep association of fluorophor with micelle
(iv) $M_Q{\cdot}F + F \underset{2k_{-b}}{\overset{k_b}{\rightleftharpoons}} M_Q{\cdot}F_2$	
(v) $M_Q{\cdot}F_{n-1} + F \underset{nk_{-b}}{\overset{k_b}{\rightleftharpoons}} M_Q{\cdot}F_n$	
(vi) $M_Q{\cdot}F_n + h\nu \xrightarrow{\chi_m I_a} M_Q{\cdot}F^*{\cdot}F_{n-1} \xrightarrow{Nk'_q} M_Q{\cdot}F_n$	excitation of micelle-phase fluorophors with subsequent static quenching
(vii) $F + h\nu \xrightarrow{\chi_a I_a} F^*$	excitation of aqueous-phase fluorophors
(viii) $Q{\cdot}F + h\nu \xrightarrow{\chi_c I_a} Q{\cdot}F^* \xrightarrow{k''_q} Q{\cdot}F$	excitation of aggregated fluorophors with subsequent static quenching
(ix) $F^* \xrightarrow{k_1} F$	first-order decays of excited fluorophors in aqueous phase
(x) $F^* + Q \xrightarrow{k_q} F + Q$	diffusional quenching of excited fluorophor by monomeric Q
(xi) $F^* + M_Q{\cdot}F_{n-1} \underset{k_{-mq}}{\overset{k_{mq}}{\rightleftharpoons}} M_Q{\cdot}F^*{\cdot}F_{n-1} \xrightarrow{Nk'_q} M_Q{\cdot}F_n$	association of excited fluorophor with micelle phase and subsequent quenching

For the case of mixed static and diffusional quenching below the cmc, as occurs with **2**-11, (4) simplifies to

$$(\Phi_0/\Phi) = (1 + K_c[Q])(1 + k_q\tau_f[Q]) \quad (6)$$

However, the fluorescence lifetime measurements indicate that $k_q\tau_f[Q] < 1$, in the concentration range covered, so that the observed fluorescence quenching below the cmc is approximated by

$$(\Phi_0/\Phi) \approx 1 + K_c[Q] \quad (7)$$

which is a description of the static quenching alone in region A. Note that K_c is only an *apparent* equilibrium constant as pointed out above. We do not wish to imply that the measured slope in region A is actually a measure of the association constant for a 1:1 complex of **2**-11 and Q.

In region B, above the cmc, static quenching of **2**-11 occurs by two independent mechanisms, and (4) reduces to

$$(\Phi_0/\Phi) = 1 + K_c\text{cmc} + K_b\{[Q]_T - \text{cmc}\}/N \quad (8)$$

Again note that $K_c$cmc is a constant and that the onset for the above relationship is revealed by the point of discontinuity in the Stern-Volmer plot which occurs at $[Q]_T$ = cmc.

Analysis of the Stern-Volmer above the cmc. The Stern-Volmer slopes in region B for **2**-1 and **2**-5 are 30 and 370 M^{-1} and the contributions from diffusional quenching (given by $k_q\tau_f$cmc) are 0.09 and 0.10, respectively. These values lead to estimates of K_b/N of 27 and 336 M^{-1} for **2**-1 and **2**-5, respectively, using eq 5. The Stern-Volmer slope in region B for **2**-11 of 3.8×10^4 M^{-1} is a direct measure of K_b/N according to (8). If N (aggregation number) for the host micelle is independent of the guest fluorophor (the indistinguishable cmc's from the three Stern-Volmer plots supports this assumption), the relative magnitudes of K_b for **2**-1:**2**-5:**2**-11 = 1.0:12:1400. Further, if a reasonable range is assumed of $60 < N < 80$,[17] the absolute values for K_b are $(1.6\text{-}2.2) \times 10^3$, $(2.0\text{-}2.7) \times 10^4$ and $(2.3\text{-}3.0) \times 10^6$ M^{-1} for **2**-1, **2**-5, and **2**-11, respectively. The strong dependence of K_b on methylene chain length in the fluorophor is in accord with known thermodynamic parameters for the distribution of hydrocarbons between organic and water phases.[18] Table II summarizes the values of the important parameters below and above the cmc.

In summary, this study indicates that fluorescence quenching of the **2**-*n* fluorophors by the surfactant nitroxyl radical **1**-Br occurs by three different mechanisms. Below the cmc, **2**-1 and **2**-5 are quenched by a simple diffusional mechanism while **2**-11 is quenched by a static mechanism. Above the cmc, static quenching of the fluorophors solubilized in the micelle phase of the surfactant nitroxyl radical becomes increasingly important, while the quenching processes involving nonmicellized quencher are expected to level off since [Q] = cmc. The relative K_b's, derived from the Stern-Volmer slopes above the cmc, vary by $\sim 10^3$ and increase, as expected, with increase in methylene chain length.

Experimental Section

Stock Solutions. All aqueous solutions used for spectroscopic measurements were prepared from commercial deionized water (<5 ppm) that was further purified by distillation from potassium permanganate. Stock solutions of **1**-Br ($\sim 10^{-3}$ M) were prepared and diluted as needed. Some crystallization occurs after several days with solutions containing $\gtrsim 10^{-3}$ M **1**-Br, which can be redissolved upon sonication. The UV-vis absorption spectra of these stock solutions do not change over several weeks. Stock solutions containing **2**-1, **2**-5, and **2**-11 ($\sim 10^{-4}$ M in water) were prepared and used as needed. The exact concentrations of these fluorophors in the precipitate-free final solutions were determined by UV-vis absorption spectroscopy.

ESR Spectra and Intensity Measurements. All spectra were re-

Table II. Stern-Volmer Slopes and Important Derived Parameters

system	Stern-Volmer slopes, M^{-1} region A	region B	derived values $k_q \times 10^{-9}$, M^{-1} s^{-1}	K_b/N, M^{-1}
2-1	~200[a]	30	~4	27
2-5	220[a]	370	~2	336
2-11	7200[b]	38000	~4[c]	38000

[a] Diffusional quenching. [b] Static quenching. [c] Obtained from lifetime measurements.

corded on a Varian E-12 X-band spectrometer equipped with a V-4532 dual cavity operated in the TE 102 mode with a resonance frequency near 9.5 GHz and a modulation frequency of 100 kHz. The sample tubes were 100-μL disposable micropipets (Corning Glass Co., no. 7099S) which show tube-to-tube reproducible signal intensity of ±5%. The intensity measurements were made relative to standard aqueous solutions of 4-keto-2,2,6,6-tetramethylpiperidinyl-*N*-oxyl (Aldrich Chemical Co.) in the second channel of the dual cavity. Identical microwave power, crystal biasing current, field-scanning rate, and modulation amplitude were used in each cavity.

Electronic Spectra. UV-vis absorption spectra were recorded on a Beckman Acta M VI spectrophotometer. Emission spectra were recorded on an American Instrument Co. spectrofluorimeter with nondegassed samples in 1-cm^2 Pyrex cuvettes.

Fluorescence Yield Measurements. Absorption and emission spectra of nondegassed aqueous solutions of **2**-1 (3×10^{-5} M), **2**-5 (3.0×10^{-5} M), and **2**-11 (1.5×10^{-5} M) were recorded in the absence and presence of varying amounts of **1**-Br. At the excitation wavelengths of 340 and 335 nm for **2**-1 and **2**-5, respectively, there was no change in absorbance with added **1**-Br. The pronounced changes in the absorption spectrum of **2**-11 with addition of **1**-Br (see text) eliminated the possibility of finding such a wavelength for that system. Accordingly an excitation wavelength of 313 nm was used and the fluorescence yields were corrected for changes in optical density at 313 nm. The maximum correction was ~30%. There was no significant absorption of incident light at the excitation wavelengths by **1**-Br in the experiments with **2**-1 and **2**-5, while this effect was <5% with **2**-11. The fluorescence yields of the latter were not corrected for this filtering. The relative fluorescence yields were determined from intensity measurements at the emission maxima of 376 and/or 395 nm and were in agreement with relative yields based on measuring the integrated area of the emissions. The error in the yield measurements is less than ±5%.

Fluorescence Lifetime Measurements. Nondegassed solutions of the fluorophors in 1-cm^2 Pyrex cuvettes were excited with the output of a pulsing nitrogen laser (337 nm, 10 ns pulse width). The emission, perpendicular to the exciting beam, was passed through a 0.5-m Bausch and Lomb monochromator set at 376 or 395 nm, onto an RCA 1P21 photomultiplier tube. The resulting signal was displayed on a Hewlett-Packard 183 oscilloscope (250 MHz) and photographically recorded. Lifetimes were determined by a least-squares fit of log (intensity) vs. time data. Exponential decays were noted over two to three lifetimes.

Synthesis of 2-1. 1-Pyrenylmethyldimethylamine. A solution of 2.3 g (0.010 M) of 1-pyrenecarboxaldehyde (Aldrich Chemical Co.) in 4.4 g (0.060 M) of dimethylformamide and 0.55 g (0.010 *M*) of formic acid was refluxed for 4 h. The excess dimethylformamide was removed in vacuo and the liquid residue was dissolved in 200 mL of anhydrous ethyl ether and filtered. Dry, gaseous hydrochloric acid was bubbled through the ether solution for several minutes and the precipitated amine salt was filtered, washed with fresh ethyl ether, and dried to yield 2.0 g of product. The amine salt was suspended in 100 mL of dry ethyl ether and neutralized by stirring for 1 h with 1 M aqueous sodium hydroxide. The ether layer was separated, dried over anhydrous magnesium sulfate, and concentrated in vacuo to yield a viscous oil which solidified upon standing. The solid was triturated with ethyl ether and filtered to give 1.5 g (60%) of yellow crystals, mp 54–56° C: NMR ($CDCl_3$) δ 8.0–8.8 (multiplet, 9 H, aromatic), 4.6 (singlet, 2 H, methylene), 2.6 (singlet, 6 H, methyl).

1-Pyrenylmethyltrimethylammonium Iodide. Excess methyl iodide was added dropwise to an ice-cold solution of the amine in dry acetone. The white precipitate was allowed to sit 1 h at 0 °C and was then filtered and washed with fresh acetone. After two recrystallizations from methanol, fine, white crystals were obtained, mp 232 °C dec. Anal. Calcd for $C_{20}H_{20}NI$: C, 59.86; H, 5.02; N, 3.49. Found: C, 59.80; H, 5.17; N, 3.69.

An aqueous solution of the iodide salt (~10^{-3} M) was ion exchanged on Amberlite IRA-400 CP to give the corresponding ammonium chloride.

Synthesis of 2-5. 5-(1-Pyrenyl)pentanoic acid was prepared as previously described,[19] mp 173–174 °C, lit. mp 165–166 °C[19] and converted into the acid chloride by standard procedures with oxalyl chloride, mp 132–135 °C.

5-(1-Pyrenyl)pentyldimethylamine. A solution of 1.60 g (0.0050 mol) of the acid chloride was dissolved in 2 mL of dry dimethylformamide and refluxed for 4 h at 150 °C. The reaction mixture was cooled and the precipitated solid was filtered, washed with 50 mL of water, suction filtered, dissolved in chloroform, and dried over anhydrous magnesium sulfate. The mixture was filtered and the solvent removed in vacuo yielding the *N*,*N*-dimethylamide as a pale yellow powder (1.2 g, 70%): mp 85–87 °C; IR ($CHCl_3$) 1635 cm^{-1} (s, C=O); NMR ($CDCl_3$) δ 7.8–8.3 (multiplet, 9 H, aromatic), 3.38 (t, 2 H, 1-Py-CH_2-), 2.95, 2.93 (d, 6 H, -$CON(CH_3)_2$), 2.36 (t, 2 H, -CH_2CO-), 1.87 (multiplet, 4 H, -CH_2CH_2-).

A solution of 2.4 g (0.010 mol) of the amide in 50 mL of anhydrous ethyl ether was added dropwise to a stirred suspension of 0.38 g (0.010 mol) of lithium aluminum hydride in 10 mL of anhydrous ethyl ether. The mixture was stirred and refluxed for 24 h. After cooling to room temperature, 10 mL of water was added dropwise with stirring, followed by a cold solution of 5 g of sodium hydroxide in 10 mL of water. The ether phase separated and the aqueous phase was extracted with fresh ethyl ether. The combined ether extracts were dried over potassium pellets. Concentration of the filtered ether extracts yielded 1.2 g (50%) of the amine as a clear oil: NMR ($CDCl_3$) δ 7.8–8.3 (multiplet, 9 H, aromatic), 3.33 (t, 2 H, 1-Py-CH_2-), 2.22 (s, 6 H, -$N(CH_3)_2$), 2.3 (t, 2 H, -CH_2-N), 1.8 (broad multiplet, 2 H, -$CH_2CH_2CH_2$-), and 1.4–1.6 (broad multiplet, 4 H, -CH_2CH_2-).

5-(1-Pyrenyl)pentyltrimethylammonium Iodide and Chloride. The ammonium iodide was readily prepared by addition of excess methyl iodide to a concentrated ethyl ether solution of the secondary amine at 0 °C. The precipitated salt was filtered and recrystallized from ethanol/benzene to give needle sharp white crystals, mp 178–179 °C. Anal. Calcd for $C_{24}H_{28}NI$: C, 63.02; H, 6.17; N, 3.06. Found: C, 61.81; H, 6.11; N, 2.96. NMR ($CDCl_3/CD_3SOCD_3$, 4/1): δ 7.8–8.3 (multiplet, 9 H, aromatic), 3.4 (two superpositioned triplets, 4 H, 1-Py-CH_2-, -CH_2-N^+), 3.22 (s, 9 H, -$N(CH_3)_3$), 2.6 (multiplet, 6 H, -$CH_2CH_2CH_2$-).

An aqueous solution of the chloride salt was obtained by ion-exchange chromatography of aqueous solution of the iodide salt on Amberlite IRA-400. The exact concentration of **2**-5 in the resulting solution was determined by UV-vis absorption spectroscopy.

Synthesis of 2-11. 11-Bromoundecanoyl chloride was prepared by conventional means from 11-bromoundecanoic acid.

11-Keto-11-(1-pyrenyl)undecanyl Bromide. To a magnetically stirred ice-cold solution of 20 g (0.071 mol) of 11-bromoundecanoyl chloride and 17 g (0.085 mol) of pyrene in 200 mL of 1,2-dichloroethane was added in small portions over 15 min 11 g (0.085 mol) of anhydrous aluminum chloride. The reaction mixture was allowed to warm to room temperature and was stirred for 24 h and then poured into 300 mL of water. The aqueous phase was saturated with sodium chloride, 300 mL of fresh, 1,2-dichloroethane was added and the organic and water layers were separated. The organic layer was washed with a saturated sodium chloride solution, dried over anhydrous magnesium sulfate, filtered, and concentrated in vacuo to give 28 g (90%) of a greenish yellow solid: mp 60–62 °C; IR (CCl_4) ν_{CO} 1675 cm^{-1}; NMR ($CDCl_3$) δ 7.8–8.2 (multiplet, 9 H, aromatic), 3.3 (triplet, 2 H, methylene), 3.1 (triplet, 2 H, methylene), 1.2–2.0 (broad, 16 H, -$(CH_2)_8$-).

11-Keto-11-(1-pyrenyl)undecanyltrimethylammonium Bromide. To an ice-cold solution of 10 g (0.020 mol) of 11-keto-11-(1-pyrenyl)-undecanyl bromide in 100 mL of a 75:25 ethyl ether/benzene mixture was added 4.8 g (0.080 mol) of chilled trimethylamine. The mixture was kept at 5 °C for several days. The precipitate was filtered to give 7.0 g of a pale yellow powder. Recrystallization from methanol–benzene yielded fine, pale yellow crystals, mp 171–172 °C. Anal. Calcd for $C_{30}H_{38}NOBr$: C, 70.85; H, 7.53; N, 2.76. Found: C, 69.53; H, 7.21; N, 2.42.

11-(1-Pyrenyl)undecanyltrimethylammonium Bromide. A mixture of 7.2 g of mossy zinc, 0.72 g of mercuric chloride, 0.5 mL of con-

centrated hydrochloric acid and 15 mL of water was stirred for 5 min. The solution was decanted and 2.6 g (0.005 mol) of the previously prepared ketone precursor was added to the amalgamated zinc followed by 12 mL of concentrated hydrochloric acid and 5 mL of water. The mixture was refluxed for 48 h and 4 mL of fresh concentrated hydrochloric acid was added every 8 h. The hot solution was filtered off from the remaining zinc and cooled and the precipitated pale, yellow crystals were filtered (1.0 g, 40%). Recrystallization from methanol gave fine, granular, pale yellow crystals: mp 182–184 °C; NMR ($CDCl_3/CD_3SOCD_3$, 3/1) δ 7.8–8.4 (multiplet, 9 H, aromatic), 3.35 (two superimposed triplets, 4 H, $-CH_2-N^+$ and 1-pyrenyl-CH_2-), 3.1 (singlet, 9 H, $-N^+(CH_3)_3$), 1.2–2.0 (broad, 18 H, $-(CH_2)_9-$).

Appendix

From Scheme I, where $\Sigma_{n=1}^{\infty}[M_Q{\cdot}F_{n-1}] = [M_Q]_T$ and $\Sigma_{n=1}^{\infty}[M_Q{\cdot}F^*{\cdot}F_{n-1}] = [M_Q{\cdot}F^*]$[20] and assuming $NK_q' \gg k_{-mq}'$, $d[F^*]/dt = \chi_a I_a - (k_1 + k_q[Q] + k_{mq}[M_Q]_T)[F^*]$, where $\chi_a = [F]/([F] + [F{\cdot}Q] + [M_Q{\cdot}F])$, which at the steady-state provides

$$[F^*] = \chi_a I_a \tau_a \qquad (a)$$

where $\tau_a = (k_1 + k_{mq}[M_Q]_T + k_q[Q])^{-1}$. Note that [Q] varies between zero and the cmc, and is a constant above the cmc. Recognizing that static quenching occurs for the excited species $M_Q{\cdot}F^*$ and $F^*{\cdot}Q$, the fluorescence quantum yield is given by

$$\Phi = \Phi_a = k_f[F^*]/I_a = k_f\chi_a\tau_a \qquad (b)$$

Since $\Phi^\circ = k_f\tau_f$

$$(\Phi_0/\Phi) = \chi_a^{-1}(\tau_f/\tau_a) = \chi_a^{-1}\tau_f(k_1 + k_{mq}[M_Q]_T + k_q[Q]) \qquad (c)$$

Since $k_{mq}[M_Q]_T\tau_f \approx 0$, (c) simplifies to

$$(\Phi_0/\Phi) = \chi_a^{-1}(1 + k_q\tau_f[Q]) \qquad (d)$$

Recognizing that $\chi_a = [F]/[F]_T$, where $[F]_T$ is the total fluorophor concentration, gives

$$(\Phi_0/\Phi) = ([F]_T/[F])(1 + k_q\tau_f[Q]) \qquad (e)$$

From the multistep equilibrium for association of the fluorophor with the micelle phase

$$[F]_T = [F] + [Q{\cdot}F] + \sum_{n=1}^{\infty} n[M_Q{\cdot}F_n] \qquad (f)$$

We have previously shown that the multistep equilibrium leads to[5b]

$$[F]_T = [F] + [Q{\cdot}F] + K_b[M_Q][F]e^{\{K_b[F]\}} \qquad (g)$$

Similarly

$$[M_Q]_T = [M_Q] + \sum_{n=1}^{\infty}[M_Q{\cdot}F_n] \qquad (h)$$

where

$$[M_Q]_T = [M_Q]e^{\{K_b[F]\}} \qquad (i)$$

Substituting (i) into (g) gives

$$[F]_T = [F] + [Q{\cdot}F] + K_b[F][M_Q]_T \qquad (j)$$

which directly leads to

$$[F]_T/[F] = 1 + [Q{\cdot}F]/[F] + K_b[M_Q]_T \qquad (k)$$

From step ii in Scheme I, it follows that

$$[F]_T/[F] = 1 + K_c[Q] + K_b[M_Q]_T \qquad (l)$$

which when substituted into (e) gives

$$(\Phi_0/\Phi) = (1 + K_c[Q] + K_b[M_Q]_T)(1 + k_q\tau_f[Q]) \qquad (m)$$

Equation m is the comprehensive Stern–Volmer relation that takes into account static quenching by Q and M_Q and diffusional quenching by Q.

References and Notes

(1) (a) G. Radda and J. Vanderkooi, *Biochim. Biophys. Acta*, **265**, 509 (1972); (b) A. Azzi, *Q. Rev. Biophys.*, **8**, 237 (1975); (c) J. H. Fendler and E. J. Fendler, "Catalysis in Micellar and Macromolecular Systems", Academic Press, New York, 1975; (d) J. K. Thomas, *Acc. Chem. Res.*, **10**, 133 (1977), and references therein; (e) M. W. Geiger and N. J. Turro, *Photochem. Photobiol.*, **26**, 221 (1977), and references therein; (f) R. C. Dorrance and T. F. Hunter, *J. Chem. Soc., Faraday Trans. 1*, **74**, 1891 (1978), and references therein; (g) G. D. Correll, R. N. Cheser, III, F. Nome, and J. H. Fendler, *J. Am. Chem. Soc.*, **100**, 1254 (1978).

(2) S. Atik and L. A. Singer, *J. Am. Chem. Soc.*, **100**, 3234 (1978).

(3) (a) J. A. Green, II, L. A. Singer, and J. H. Parks, *J. Chem. Phys.*, **58**, 2690 (1973); (b) *J. Am. Chem. Soc.*, **96**, 2730 (1974).

(4) S. Atik and L. A. Singer, *Chem. Phys. Lett.* **59**, 519 (1978).

(5) (a) For a general discussion of the ESR spectroscopy of nitroxyl radicals with application of spin-labeling experiments, see L. J. Berliner, Ed., "Spin Labeling. Theory and Applications", Academic Press, New York, 1976. (b) For our earlier study of the binding of **1**-Cl to the cetyltrimethylammonium chloride micelle, see C. L. Kwan, S. Atik, and L. A. Singer, *J. Am. Chem. Soc.*, **100**, 4783 (1978). (c) For ESR studies on structurally similar nitroxide radicals, see K. K. Fox in "Chemical and Biological Applications of Relaxation Spectrometry", E. Wyn-Jones, Ed., D. Reidel Publishing Co., Boston, Mass., 1975, p 215.

(6) Hereafter, "static quenching" means quenching that occurs with fluorophors already associated with the quencher in the ground state, while "diffusional quenching" is by collisional or diffusion-controlled encounter between the excited fluorophor and quencher.

(7) The surface tension of aqueous solutions of **1**-Br at 25 °C decreases sharply with increasing concentration (e.g., at 5.0×10^{-5} M, γ is 53.6 dynes/cm) until a minimum value of 37.5 dynes/cm is reached at $\sim 3 \times 10^{-4}$ M. Above that concentration, the surface tension very nearly is constant (e.g., at 6×10^{-4} and 1.5×10^{-3} M, γ is 44.0 and 43.0 dynes/cm, respectively). The region of discontinuity in the surface tension measurements ($\sim 4 \times 10^{-4}$ M) agrees well with the ESR estimate of the cmc of **1**-Br.

(8) From the Gibb's equation. See A. W. Adamson, "The Physical Chemistry of Surfaces", 3rd ed., Wiley, New York, 1976.

(9) M. F. Emerson and A. Holtzer, *J. Phys. Chem.*, **71**, 1898 (1967).

(10) P. H. Elworthy, A. T. Florence, and C. B. MacFarlane, "Solubilization by Surface Active Agents", Chapman and Hall Ltd., London, 1968, pp 48–51.

(11) J. B. Birks, "Photophysics of Aromatic Molecules", Wiley-Interscience, New York, 1970, p 301.

(12) The observed aqueous phase diffusional quenching and micelle phase static quenching is not by Br^-. The fluorescence lifetime of **2**–5 in the presence of 0.0050 M NaBr is decreased only to $\tau_{obsd} = 99$ ns which indicates $k_q = 6 \times 10^7\ M^{-1}\ s^{-1}$ which is about 20-fold less than k_q's for nitroxyl radical quenching from this and other[3] studies. We measure the fluorescence lifetime of **2**-5 solubilized in the cetyltrimethylammonium bromide (CTAB) micelle as 90 ns compared with 123 ns in the cetyltrimethylammonium chloride (CTAC) micelle. Assuming that fluorescence quenching by Cl^- in the latter micelle host is negligible, it follows that $\tau_{CTAB}^{-1} - \tau_{CTAC}^{-1} = nk_q' \approx 3 \times 10^6\ s^{-1}$, where k_q' is the rate constant for intramicellar fluorescence quenching by Br^- ions associated with a single micelle, and n is the number of Br^- ions. With the reasonable approximation that $10 < n < 100$, $k_q' \approx 10^4$ to $10^5\ s^{-1}$, which is two or three orders of magnitude smaller than the k_q', we recently measured for fluorescence quenching of pyrene by **1** in a CTAC micelle host.[4]

(13) Note that the Stern–Volmer slope of 400 M^{-1} means that for the diffusional mechanism $(\Phi_0/\Phi) \approx 1.2$ at $[Q] = 4 \times 10^{-4}$ M (17% quenching), while the observed value is $(\Phi_0/\Phi) = 4.0$ (75% quenching).

(14) The cmc of CTAC by surface tension measurements is $\sim 4 \times 10^{-3}$ M in the presence of 2.5×10^{-5} M **2**-11 which agrees with our previous ESR measurement[5b] in the absence of added fluorophor.

(15) See T. Kawahima, T. Otsubo, Y. Sakata, and S. Misumi (*Tetrahedron Lett.*, 5115 (1978)) for a discussion of the effect of the stacking mode of two pyrene rings on the electronic absorption and emission spectra of several [2.2]pyrenophanes.

(16) In our previous study,[4] we show that intramicellar fluorescence quenching is given by Nk_q', where N is the number of quenchers in the same host micelle as the fluorophore, and k_q' is the quenching rate constant in units of s^{-1}. Using the fluorescence lifetime of these fluorophors in a CTAC micelle ($\sim$100 nsec) as an indication of k_1', along with the previously measured $k_q' \approx 1 \times 10^7\ s^{-1}$ for fluorescence quenching of pyrene by 1, and assuming an aggregation number of $\sim$60,[17] indicates $Nk_q' \gg k_1'$.

(17) This estimate is based on the likely range of $60 < N < 80$ for the similarly structured CTAC micelle. P. Mukerjee and K. Mysels, "Critical Micelle Concentrations of Surfactant Systems", National Bureau of Standards reference Data Series, National Bureau of Standards, Washington, D.C., 1971.

(18) C. Tanford, "The Hydrophobic Effect: Formation of Micelles and Biological Membranes", Wiley-Interscience, New York, 1973.

(19) O. Perin-Roussel, N. P. Buu-Hoi, and P. Jacquinon, *Bull. Soc. Chim. Fr.*, 2160 (1971).

(20) Intramicellar excimer[11] formation is excluded from the derivation that follows since it would introduce a needless complication. Although excimer formation, in principle, could occur in $M_Q{\cdot}F^*{\cdot}F_{n-1}$ where $n \geq 2$, the scheme assumes static quenching in the micelle phase so that excimer formation, as well as all other intramicellar photoprocesses, is slow relative to Nk_q'.